IEEE Access
Multidisciplinary | Rapid Review | Open Access Journal

Received December 2, 2019, accepted December 18, 2019, date of publication December 31, 2019, date of current version January 6, 2020.

Digital Object Identifier 10.1109/ACCESS.2019.2962737

Analytical and Numerical Investigation of Radiation Enhancement by Anisotropic Metamaterial Shells

R. ANEESH KUMAR[1,2], (Member, IEEE), JUSTIN G. POLLOCK[4], (Member, IEEE), CHINMOY SAHA[1], (Senior Member, IEEE), AND ASHWIN K. IYER[3], (Senior Member, IEEE)

[1]Department of Avionics, Indian Institute of Space Science and Technology, Thiruvananthapuram 695547, India
[2]Vikram Sarabhai Space Centre, Thiruvananthapuram 695022, India
[3]Electrical and Computer Engineering Department, University of Alberta, Edmonton, AB T6G1H9, Canada
[4]KP Performance Antennas Inc., Edmonton, AB T5M3X4, Canada

Corresponding author: Chinmoy Saha (chinmoy.rpe@gmail.com)

Justin Pollock and Ashwin Iyer acknowledge funding from the Natural Sciences and Engineering Research Council (NSERC) of Canada.

ABSTRACT This paper presents analytical and numerical investigations of a 3D cylindrical metamaterial shell possessing a cylindrically anisotropic permeability that is excited by a finite-sized electric line source. A comprehensive field analysis of the system reveals that the compact metamaterial shell exhibits resonances akin to those observed in isotropic 2D cylindrical metamaterial structures, which may be used to enhance the radiated power of a nearby antenna. An analytical resonance condition that relates the dimensions of the cylindrical shell to its anisotropic effective-medium parameters is shown to be accurate in predicting the resonances of 2D and 3D metamaterial shells obtained using full-wave simulations. The effects of anisotropy and finite shell/antenna height on the system's near-fields, radiation patterns, and power-ratio enhancements are explored. It is shown through both theory and simulations that the condition for resonance is largely independent of shell/antenna height but that the quality factor reduces dramatically as these heights approach electrically small values. Also, a dispersion and loss analysis assuming Lorentz model is carried out, which indicates that practical metamaterial losses do not significantly degrade the power enhancement.

INDEX TERMS Anisotropic, metamaterial, radiation enhancement, power ratio, resonance condtion.

I. INTRODUCTION

Metamaterials are extensively being explored to enhance the radiation characteristics of microwave antennas. Antennas with enhanced radiated power are an essential requirement in improving the quality of microwave communication especially for long-distance applications. Metamaterials were shown to modify the emission of a point source, where the source is embedded inside an isotropic zero index material [1], in which was reported enhancement of directivity. Directivity enhancement using anisotropic metamaterials with one component of permeability/permittivity tensor near zero [2], [3] was also demonstrated. A horn antenna filled with bulk anisotropic metamaterial [4] as well as a planar bow tie end-fire radiator placed near an array of split ring resonators [5] were also shown to have enhanced gain. Apart from such bulk-metamaterial-based gain enhancement, several works have studied gain enhancement using metasurfaces [6]–[12]. But all these works focus on gain enhancement of radiating structures using near-zero physical properties rather than enhancement of total radiated power.

Several studies have reported radiated power enhancement using metamaterial shells over last decade. Analytical studies have shown that line sources adjacent to 2D (i.e., vertically infinite) isotropic, homogenous cylindrical structures (or shells) possessing single-negative (SNG) or double-negative (DNG) effective-medium properties may produce a dramatic improvement in radiated power [13]. Radiated power enhancement has also been observed when enclosing a line source with dielectric rod in a radially anisotropic zero-index metamaterial (RAZIM) shell [14]. But such a structure enables radiation enhancement of only omnidirectional

The associate editor coordinating the review of this manuscript and approving it for publication was Shah Nawaz Burokur.

radiation, by rescattering of the anisotropic higher order cylindrical modes trapped in the shell as the isotropic 0-th order mode. However, many practical applications require radiation in particular directions. Accordingly, enhancement in radiated power with directional patterns have also been demonstrated, but these devices rely on to the coupling to, and excitation of, structural resonances in SNG/DNG shells that can occur at much lower frequencies than those of shells composed of natural dielectrics [13], [15]. Such resonances are highly sensitive to the physical dimensions and constitutive parameters of the effective medium. A resonance condition relating the physical dimensions of a cylindrical metamaterial shell excited by an ELS to its isotropic effective-medium properties was reported by Arslanagić *et al.* [16]. A Hertzian dipole placed inside concentric metamaterial spheres are also shown to exhibit enhancements in its radiated power when a resonance condition relating the sphere's radius to its constituent isotropic material parameters is satisfied [21]. But a spherical metamaterial must fully encompass the antenna, which presents both fabrication/integration challenges.

All the above mentioned work in the directional enhancement of radiated power with structural resonances employ isotropic effective media, which may not be realistic, given that most metamaterials exhibit some degree of anisotropy. This calls for a detailed study on structural resonances in anisotropic DNG/SNG media and their effect on radiated power. However, employing anisotropic metamaterial shells in practical settings and applications faces various challenges, including designing the anisotropic material parameters of the metamaterial shell at the antenna operating frequency, and positioning and orientation of a practical excitation source to create the required field polarizations to effect the resonances. Furthermore, since the resonance phenomenon in the analysis of the 2D isotropic metamaterial shell is extremely sensitive to its dimensions and constitutive parameters, a complete and robust analysis of 3D anisotropic metamaterial shells considering finite height is necessary to encourage their adoption in real-world applications. For instance, it could aid in designing novel miniaturized dielectric resonator antennas (DRA) [22], such as the epsilon-near-zero (ENZ) compact antenna [23]. Research works have also presented the improvement in radiated power of antennas placed next to radial arrangements of transmission-line (TL) metamaterials [17], capacitively-loaded-loops [18], and radial photonic crystal shells [19]. All these works demonstrate the need to build upon these isotropic models and consider the effects of anisotropy, which are prevalent in all practical cylindrical arrangements of metamaterials [20].

In this work, we first analytically study the structural resonances in an anisotropic SNG/DNG medium and derive a commensurate resonance condition which relates the physical dimension of the shell to anisotropic tensor elements. The derivation of such a resonance condition is no trivial task and to the best of the authors' knowledge, no such analysis on resonances in anisotropic metamaterial shells and their associated resonance condition is available in the open literature. Furthermore, as will be shown in this work, there is strong evidence to suggest that the resonances are strongly dominated by the metamaterial shell's response transverse to its axis, making it akin to a 2D system. This helps to simplify the model and aid in the derivation of approximate resonance condition. Extensive numerical studies, both in 2D and a more practical 3D case, are then conducted to validate the resonance condition in design of anisotropic structures to excite structural resonances and study the effect of such resonances in enhancement of radiated power. It is found that the resonance condition provides an approximate solution in the case of long metamaterial shells but deviates significantly in the case of short shells. The effects of dispersion and loss on radiation enhancement of such 3D anisotropic shells are also studied.

This paper is organized as follows: Sec.II presents a detailed mathematical analysis of the metamaterial shell whose permittivity and permeability tensors possess radial, azimuthal and axial components, and which is excited by a finite-sized ELS. Section III investigates the radiation performance of a simplified 2D anisotropic metamaterial shell excited by an ELS possessing a uniform current using full-wave simulations and explores the effect of anisotropy on the radiated power. This investigation is extended to the fully 3D case of a metamaterial shell excited by a finite-sized dipole antenna, for which the implications of anisotropy and a finite height on the radiated power, near-fields, and radiation patterns are explored in Sec. IV. This study establishes that practical, finite-sized, anisotropic cylindrical metamaterials exhibit multiple structural resonances and radiated-power enhancement analogous to the theoretical observations of Ziolkowski et al. for homogeneous, isotropic metamaterial cylinders [3]. The effect of dispersion and loss on resonances of 3D anisotropic metamaterial cylinders is studied in Sec. V.

II. DERIVATION OF RESONANCE CONDITION

The geometry of the 3D metamaterial cylindrical shell with anisotropic effective-medium properties is depicted in Fig.1.

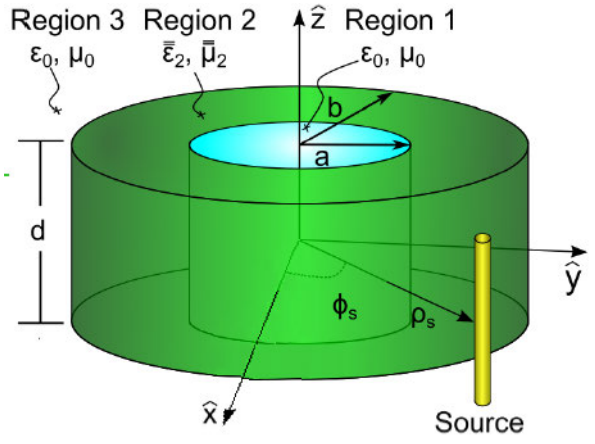

FIGURE 1. Geometry of the 3D anisotropic metamaterial shell excited by a *z*-directed ELS.

It consists of an inner vacuum region (Region 1) of radius a that is surrounded by an anisotropic metamaterial shell (Region 2) of radius b and height d, which is embedded in a vacuum region (Region 3). Region 2 possesses anisotropic material parameters that are described by tensors diagonalized in a cylindrical coordinate system. Taking the coordinate-system axes to coincide with the shell axes, these take the form $\bar{\bar{\epsilon}} = \bar{\bar{I}}(\epsilon_\rho, \epsilon_\phi, \epsilon_z)$ and $\bar{\bar{\mu}} = \bar{\bar{I}}(\mu_\rho, \mu_\phi, \mu_z)$ in which $\bar{\bar{I}}$ is the identity dyadic. A z-directed ELS of height d is centered at $(\rho_s, \phi_s, z = 0)$ and illuminates the anisotropic metamaterial shell. For the time being, this study neglects the impact of material losses and assumes the material parameters have no imaginary component. The perturbation introduced by practical losses is studied numerically in Sec. V.

A field and dispersion analysis accounting for the full 3D shell excited by a practical source is numerically cumbersome and it is difficult to gain design intuition from the resulting complicated formulation [24]. Instead, its response is more easily obtained using numerical methods or through making a number of approximations that simplify the problem without offending the underlying physical phenomena. Here, a modified Itoh and Rudokas model [24] is employed, which has proven accurate in predicting the resonance frequencies of cylindrical DRAs, and assumes that the scattered fields from the metamaterial shell at resonance will be strongly concentrated within $|z| < d/2$ with exponential decay for $|z| > d/2$. In this work, it is further assumed for simplicity that the fields are effectively zero in the region $|z| > d/2$. This can be modeled by applying an infinite perfect electric conductor (PEC) surface extending over the planes $z = \pm d/2$.

The generally inhomogeneous nature of the metamaterial-shell system suggests that the resonator supports hybrid electric *HE* and hybrid magnetic *EH* modes in which axial (z-directed) electric and magnetic fields generally exist. However, we assume that the dominant *TM* field polarization of the z-directed ELS allows us to neglect the hybrid nature of the modes such that the total fields can be expressed with the *TM* field components (E_ρ, E_ϕ, E_z) and $(H_\rho, H_\phi, H_z = 0)$. In order to generate the fields of this *TM* mode, we require a magnetic vector potential which takes the form,

$$\bar{A} = \hat{z}A_z = \hat{z}A_0 g(k_\rho \rho)\cos(n\phi) f(k_z z) \tag{1}$$

where A_0 is a constant, k_ρ and k_z are the components of the propagation constant in the ρ- and z- directions, respectively, and g and f are general functions representing the ρ- and z- variation of the fields, respectively. Whereas the enforced PEC boundary condition stipulates that f varies sinusoidally for $|z| < d/2$, the function g can be represented as combinations of Bessel functions of the 1st and 2nd kind whose exact form varies in each region. The constant A_0 is derived from Ampere's law by considering that the ELS supports a current with a maximum amplitude I_e, which can be related to A_z according to

$$I_e = \lim_{\rho \to 0} \int_0^{2\pi} (H_\phi)_{max} \rho d\phi \tag{2a}$$

$$\text{where} \quad (H_\phi)_{max} = \left(-\frac{1}{\mu_\phi}\frac{\partial A_z}{\partial \rho}\right)_{max} \tag{2b}$$

yielding $A_0 = -j\mu_\phi I_e/4$. The ρ, ϕ, and z components of the electric field are related to A_z by [25],

$$E_\rho = -j\frac{1}{\omega\epsilon_\rho\mu_\phi}\frac{\partial^2 A_z}{\partial\rho\partial z} \tag{3a}$$

$$E_\phi = -j\frac{1}{\omega\epsilon_\phi\mu_\rho}\frac{1}{\rho}\frac{\partial^2 A_z}{\partial\phi\partial z} \tag{3b}$$

$$E_z = \frac{j}{\omega\epsilon_z\mu_\phi}\frac{1}{\rho}\frac{\partial}{\partial\rho}\left(\rho\frac{\partial A_z}{\partial\rho}\right) + \frac{j}{\omega\epsilon_z\mu_\rho}\frac{1}{\rho^2}\frac{\partial^2 A_z}{\partial\phi^2} \tag{3c}$$

$$H_\rho = \frac{1}{\mu_\rho}\frac{1}{\rho}\frac{\partial A_z}{\partial\phi} \tag{3d}$$

$$H_\phi = -\frac{1}{\mu_\phi}\frac{\partial A_z}{\partial\rho} \tag{3e}$$

to give,

$$E_\rho = \frac{I_e k_\rho k_z}{4\omega\epsilon_\rho} g'(k_\rho\rho)\cos(n\phi) f'(k_z z) \tag{4a}$$

$$E_\phi = \frac{I_e n\mu_\rho k_z}{4\omega\epsilon_\phi\mu_\rho\rho} g(k_\rho\rho)\sin(n\phi) f'(k_z z) \tag{4b}$$

$$E_z = \frac{-I_e k_\rho^2}{4\omega\epsilon_z} g(k_\rho\rho)\cos(n\phi) f(k_z z) \tag{4c}$$

$$H_\rho = \frac{j\mu_\phi n}{4\mu_\rho\rho} g(k_\rho\rho)\sin(n\phi) f'(k_z z) \tag{4d}$$

$$H_\phi = \frac{jI_e k_\rho}{4} g'(k_\rho\rho)\cos(n\phi) f(k_z z) \tag{4e}$$

where $k_\rho^2 = k_0^2\epsilon_z\mu_\phi - \frac{\mu_z}{\mu_\rho}k_z^2$ and $k_0 = \frac{\omega}{c}$ is the free-space propagation constant.

The ELS is displaced from the origin to a position (ρ_s, ϕ_s), which requires invocation of the addition theorems to represent the fields using a cylindrical-wave expansion. The z component of the electric field and ϕ component of the magnetic field generated by the ELS will take the form,

$$E_{zi}^{ELS} = -I_e\frac{k_{\rho i}^2}{4\omega\epsilon_i} f(k_{zi} z) \sum_{n=-N}^{N} J_m(k_{\rho i}\rho) H_m^{(2)}(k_{\rho i}\rho_s)\exp^{jn(\phi-\phi_s)}, \quad \rho < \rho_s \tag{5a}$$

$$E_{zi}^{ELS} = -I_e\frac{k_{\rho i}^2}{4\omega\epsilon_i} f(k_{zi} z) \sum_{n=-N}^{N} J_m(k_{\rho i}\rho_s) H_m^{(2)}(k_{\rho i}\rho)\exp^{jn(\phi-\phi_s)}, \quad \rho > \rho_s \tag{5b}$$

$$H_{\phi i}^{ELS} = \frac{jI_e k_{\rho i}}{4} f(k_{zi} z) \sum_{n=-N}^{N} J_m'(k_{\rho i}\rho) H_m^{(2)}(k_{\rho i}\rho_s)\exp^{jn(\phi-\phi_s)}, \quad \rho < \rho_s \tag{5c}$$

$$H_{\phi i}^{ELS} = \frac{jI_e k_{\rho i}}{4} f(k_{zi} z)$$

$$\sum_{n=-N}^{N} J'_m(k_{\rho i}\rho_s)H_m^{(2)}(k_{\rho i}\rho)\exp^{jn(\phi-\phi_s)}, \quad \rho > \rho_s \quad (5d)$$

where $m = n\sqrt{\mu_{\phi 2}/\mu_{\rho 2}}$, i = 1,2,3 refers to the region in which the ELS is located, and N represents the maximum azimuthal mode number included in the cylindrical-wave expansion (finite for numerical evaluation). The scattered fields can then be expressed as,

$$E^s_{z1} = -I_e \frac{k^2_{\rho 1}}{4\omega\epsilon_0} f(k_{z1}z) \sum_{n=-N}^{N} C_{1n} J_n(k_{\rho 1}\rho) e^{jn(\phi-\phi_s)} \quad (6a)$$

$$E^s_{z2} = -I_e \frac{k^2_{\rho 2}}{4\omega\epsilon_z} f(k_{z2}z) \sum_{n=-N}^{N} (C_{2n} J_m(k_{\rho 2}\rho) + C_{3n} Y_m(k_{\rho 2}\rho)) e^{jn(\phi-\phi_s)} \quad (6b)$$

$$E^s_{z3} = -I_e \frac{k^2_{\rho 3}}{4\omega\epsilon_0} f(k_{z3}z) \sum_{n=-N}^{N} C_{4n} H_n^2(k_{\rho 3}\rho) e^{jn(\phi-\phi_s)} \quad (6c)$$

$$H^s_{\phi 1} = \frac{jI_e k_{\rho 1}}{4} f(k_{z1}z) \sum_{n=-N}^{N} C_{1n} J'_n(k_{\rho 1}\rho) e^{jn(\phi-\phi_s)} \quad (6d)$$

$$H^s_{\phi 2} = \frac{jI_e k_{\rho 2}}{4} f(k_{z2}z) \sum_{n=-N}^{N} (C_{2n} J'_m(k_{\rho 2}\rho) + C_{3n} Y'_m(k_{\rho 2}\rho)) e^{jn(\phi-\phi_s)} \quad (6e)$$

$$H^s_{\phi 3} = \frac{jI_e k_{\rho 3}}{4} f(k_{z3}z) \sum_{n=-N}^{N} C_{4n} H_n^{'(2)}(k_{\rho 3}\rho) e^{jn(\phi-\phi_s)} \quad (6f)$$

Using (4a)-(4e), the remaining field components can be derived. The continuity of the tangential electric- and magnetic-field components at $\rho = a$ and $\rho = b$ relate the coefficients $\bar{Cn} = C_{1n}, C_{2n}, C_{3n}, C_{4n}$ in matrix form as $\bar{M}_n\bar{C}_n = \bar{D}_n$ where, $\bar{M}_n$ is given by (7), as shown at the bottom of this page, and $\bar{D}_n$ is given by (8), as shown at the bottom of this page.

The resonances of the metamaterial shell are determined by solving $det(\bar{M}_n) = 0$. Although not shown, the determinant of (7) consists of products of Bessel, Neumann, and Hankel functions, and, in general, must be solved numerically. However, by enforcing the condition that the metamaterial shell is electrically small (i.e., $k_{\rho i}a \ll 1$ and $k_{\rho i}b \ll 1$), the determinant can be simplified using small-argument approximations as follows:

$$J_m(k_{\rho 2}a)Y_m(k_{\rho 2}b) = \frac{-1}{m\pi}\left(\frac{a}{b}\right)^m \quad (9a)$$

$$J'_m(k_{\rho 2}a)Y_m(k_{\rho 2}b) = \frac{-1}{k_{\rho 2}a\pi}\left(\frac{a}{b}\right)^m \quad (9b)$$

$$J_m(k_{\rho 2}a)Y'_m(k_{\rho 2}b) = \frac{-1}{k_{\rho 2}b\pi}\left(\frac{a}{b}\right)^m \quad (9c)$$

$$J'_m(k_{\rho 2}a)Y'_m(k_{\rho 2}b) = \frac{m}{\pi}\frac{1}{k^2_{\rho 2}}\frac{1}{ab}\left(\frac{a}{b}\right)^m \quad (9d)$$

$$J'_n(k_{\rho 1}a) = \frac{n}{k_{\rho 1}a}J_n(k_{\rho 1}a) \quad (9e)$$

$$H_n^{'2}(k_{\rho 3}b) = \frac{n}{k_{\rho 3}b}H_n^{*2}(k_{\rho 3}b) \quad (9f)$$

where the asterisk (*) denotes the complex conjugate. Applying (9a)-(9f) to $det(\bar{M}_n) = 0$ gives,

$$\frac{J_n(k_{\rho 1}a)f^4(k_{z0}z)}{\pi ab}\Big[\Big(\frac{mk^4_{\rho 0}(\frac{b}{a})^m}{\epsilon_0^2} - \frac{mk^4_{\rho 0}(\frac{a}{b})^m}{\epsilon_0^2} + \frac{nk^2_{\rho 2}k^2_{\rho 0}(\frac{a}{b})^m}{\epsilon_0\epsilon_{z2}} + \frac{nk^2_{\rho 2}k^2_{\rho 0}(\frac{b}{a})^m}{\epsilon_0\epsilon_{z2}}\Big)H_n^2(k_{\rho 3}b) \Big(-\frac{nk^2_{\rho 2}k^2_{\rho 0}(\frac{a}{b})^m}{\epsilon_0\epsilon_{z2}} - \frac{nk^2_{\rho 2}k^2_{\rho 0}(\frac{b}{a})^m}{\epsilon_0\epsilon_{z2}} + \frac{nk^4_{\rho 2}(\frac{a}{b})^m}{\sqrt{\frac{\mu_{\phi 2}}{\mu_{\rho 2}}}\epsilon^2_{z2}} - \frac{nk^4_{\rho 2}(\frac{b}{a})^m}{\sqrt{\frac{\mu_{\phi 2}}{\mu_{\rho 2}}}\epsilon^2_{z2}}\Big)H_n^{*2}(k_{\rho 3}b)\Big] = 0 \quad (10)$$

Equation (10) suggests that the determinant of $\bar{M}_n$ can be made zero if either $J_n(k_{\rho 1}a) = 0$ or $f^4(k_{z0}z) = 0$, or if the entire factor in the brackets is zero. It is worth noting that (10) suggests that resonances are formed in the transverse (ρ-ϕ) plane and in the longitudinal (z-) direction. In fact, the transverse resonances are independent of height, which suggests that they are strongest when $k_z = 0$. Under this condition, the term in the brackets reduces to,

$$\frac{a}{b} \approx \left(\frac{\mu_{\phi 2} + \mu_0\sqrt{\frac{\mu_{\phi 2}}{\mu_{\rho 2}}}}{\mu_{\phi 2} - \mu_0\sqrt{\frac{\mu_{\phi 2}}{\mu_{\rho 2}}}}\right)^{1/m} \quad (11)$$

$$\bar{M}_n = \begin{bmatrix} -\frac{k^2_{\rho 1}}{\epsilon_0}f(k_{z1}z)J_n(k_{\rho 1}\,a) & \frac{k^2_{\rho 2}}{\epsilon_{z2}}f(k_{z2}z)J_m(k_{\rho 2}\,a) & \frac{k^2_{\rho 2}}{\epsilon_{z2}}f(k_{z2}z)Y_m(k_{\rho 2}\,a) & 0 \\ k_{\rho 1}f(k_{z1}z)J'_n(k_{\rho 1}\,a) & -k_{\rho 2}f(k_{z2}z)J'_m(k_{\rho 2}\,a) & -k_{\rho 2}f(k_{z2}z)Y'_m(k_{\rho 2}\,a) & 0 \\ 0 & -\frac{k^2_{\rho 2}}{\epsilon_{z2}}f(k_{z2}z)J_m(k_{\rho 2}\,b) & -\frac{k^2_{\rho 2}}{\epsilon_{z2}}f(k_{z2}z)Y_m(k_{\rho 2}\,b) & -\frac{k^2_{\rho 3}}{\epsilon_0}f(k_{z3}z)H_n^2(k_{\rho 3}\,b) \\ 0 & -k_{\rho 2}f(k_{z2}z)J'_m(k_{\rho 2}\,b) & k_{\rho 2}f(k_{z2}z)Y'_m(k_{\rho 2}\,b) & k_{\rho 3}f(k_{z3}z)H_n^{'2}(k_{\rho 3}\,b) \end{bmatrix} \quad (7)$$

$$\bar{D}_n = \begin{bmatrix} \frac{k^2_{\rho 1}}{\epsilon_0}f(k_{z1}z)J_n(k_{\rho 1}\rho_s)H_n^2(k_{\rho 1}a) \\ -k_{\rho 1}f(k_{z1}z)J_n(k_{\rho 1}\rho_s)H_n^{'2}(k_{\rho 1}a) \\ 0 \\ 0 \end{bmatrix}, \begin{bmatrix} -\frac{k^2_{\rho 2}}{\epsilon_{z2}}f(k_{z2}z)J_n(k_{\rho 2}a)H_n^2(k_{\rho 2}\rho_s) \\ -k_{\rho 2}f(k_{z2}z)J'_n(k_{\rho 2}a)H_n^2(k_{\rho 2}\rho_s) \\ \frac{k^2_{\rho 2}}{\epsilon_{z2}}f(k_{z2}z)J_n(k_{\rho 2}\rho_s)H_n^2(k_{\rho 2}b) \\ -k_{\rho 2}f(k_{z2}z)J_n(k_{\rho 2}\rho_s)H_n^{'2}(k_{\rho 2}b) \end{bmatrix}, \begin{bmatrix} 0 \\ 0 \\ -\frac{k^2_{\rho 3}}{\epsilon_0}f(k_{z3}z)J_n(k_{\rho 3}b)H_n^2(k_{\rho 3}\rho_s) \\ k_{\rho 3}f(k_{z3}z)J'_n(k_{\rho 3}b)H_n^2(k_{\rho 3}\rho_s) \end{bmatrix} \quad (8)$$

for $0 < \rho_s < a$ for $a < \rho_s < b$ for $b > \rho_s$

Equation (11) represents a resonance condition that relates the metamaterial shell's physical dimensions to its anisotropic material parameters, and is akin to the condition derived for isotropic shells [16] but differs in two important aspects: 1) the introduction of anisotropy implicates only the $\mu_{\rho 2}$ and $\mu_{\phi 2}$ components of the permeability tensor, and 2) m generally assumes complex values. Evaluation of (11) suggests that $\mu_{\phi 2} < 0$ in order to effect these resonances, which is analogous to the mu-negative (MNG) condition required by Arslanagić *et al*. for isotropic shells [16]. This allows one to relax the MNG condition on the remaining components of the permeability tensor. Furthermore, it is worth noting that (11) is independent of the permittivity. These two observations allow us to greatly simplify the design of practical cylindrical metamaterial shells. Here, $\mu_{\rho 2}$ can take on positive or negative values. Although a cursory observation of (11) suggests $\mu_{\rho 2}$ being positive while $\mu_{\phi 2}$ being negative would result in (11) being unsatisfied, we remind the reader that m in this case would be purely imaginary. As a result, the right-hand side of (11) will revert to real values. In fact, employing the complex-Gamma function to derive the small-argument approximation in (9a)-(9f), it was analytically observed that the resonance condition remains the same for both real and imaginary m. Although material losses were neglected here, (11) still provides an approximate solution when moderate material loss (such as that typical of current low-loss metamaterial technologies) is introduced. However, extreme levels of loss will, expectedly, suppress the resonances. Despite m potentially taking on complex values, (11) indicates a for each (integer) value of azimuthal order n, the first three of which are termed dipolar, quadrupolar, and sextupolar for $n = 1, 2, 3$, respectively. Despite the above assumptions, it will be shown in Secs. III-IV that the resonance condition of (11) is extremely accurate, provided the antenna's height is not electrically very small (i.e., $d \ll \lambda_0$). In this limit, the *TM* mode approximation breaks down, in that the fields can no longer be said to decay strongly for $|z| > d/2$.

Although anisotropic MNG shells are the focus of this work, duality stipulates that a similar resonance condition exists for a metamaterial shell excited by a magnetic line source (MLS). In this case, a *TE* mode approximation is used for the MLS and a PMC boundary condition is used instead on the ρ-ϕ plane at $z = \pm d/2$. Using a similar approach, the resonance condition is derived as,

$$\frac{a}{b} \approx \left(\frac{\epsilon_{\phi 2} + \epsilon_0 \sqrt{\frac{\epsilon_{\phi 2}}{\epsilon_{\rho 2}}}}{\epsilon_{\phi 2} - \epsilon_0 \sqrt{\frac{\epsilon_{\phi 2}}{\epsilon_{\rho 2}}}} \right)^{1/m'} \tag{12}$$

where, $m' = n\sqrt{\epsilon_{\phi 2}/\epsilon_{\rho 2}}$

III. NUMERICAL STUDY OF 2D ANISOTROPIC SHELLS

To gain a comprehensive understanding of the implications of anisotropy on the near- and far-fields of the ELS excited 3D metamaterial shell without considering the complications introduced by a finite height, this work first investigates the simplified 2D case. The theoretical formulation of the 2D problem can be derived from the 3D analysis by considering the case when the current is uniform along the z-axis (i.e., $f(k_z z) = 1$). Under this simplification, $k_z = 0$ (i.e., propagation is restricted to the ρ-ϕ plane), and a hybrid-mode description of the fields is no longer necessary. As a result, our original *TM* mode approximation of the fields is strictly valid for the 2D case. Therefore, our analysis suggests that only the $\mu_{\rho 2}$, $\mu_{\phi 2}$, and $\epsilon_{z 2}$ tensor elements will dictate the scattering response of the 2D metamaterial shell, which corroborates observations of similar anisotropic metamaterial shells based on TL metamaterials [17].

Full-wave simulations of the metamaterial-shell structure shown in Fig. 1 were performed using COMSOL [26], in which the simulation domain consists of a single 2D transverse (ρ-ϕ) cut. The 2D metamaterial shell is surrounded by a vacuum region of radius $\rho = 3b$ whose outer boundary is assigned as a perfectly matched layer (PML). The ELS is modeled using an infinitesimally thin PEC wire directed along the z-axis. The metamaterial shell is assigned a non-electric response $\left(\bar{\bar{\epsilon}} = \bar{\bar{I}}(1, 1, 1)\epsilon_0\right)$ and a biaxial permeability tensor with a longitudinal component $\mu_{z2} = 1$. Equation (11) indicates two possible scenarios to effect a resonance for each order n: either the ratio a/b is determined for a fixed set of material parameters or, conversely, the material parameters are determined for a fixed a/b. The latter option is more attractive in practice due to the dispersion of metamaterial parameters, which vary naturally with frequency. Accordingly, for the remainder of the paper we employ $a = 3$ mm and $b = 5$ mm with the ELS fixed at the position $\rho_s = 2.9$ mm and $\phi_s = 0^o$. Initially, we select the design frequency and carry out the analysis, assuming that one can realize the desired specific values of $\mu_{\rho 2}$ and $\mu_{\phi 2}$ at this frequency (as part of a physically appropriate dispersive response). Further, a more practical material dispersion is modeled using a Lorentz-type profile, in Sec.V. Establishing an operating frequency of 3.0 GHz, the metamaterial shell can be said to be electrically small (i.e. $k_0 b = 0.314 < 1$), which ensures that the approximations used to derive (11) are valid. This section will investigate the near-fields and the radiation enhancement of the metamaterial-shell and antenna system, which is characterized by the power ratio (PR) defined as the power radiated in the presence of the metamaterial, relative to power radiated in its absence [16]:

$$PR = 10 \log_{10} \left(\frac{P_{rad,w/metamaterial}}{P_{rad,w/ometamaterial}} \right) \tag{13}$$

Fig. 2 presents the simulated PR as a function of $\mu_{\rho 2}$ and $\mu_{\phi 2}$ for the 2D anisotropic metamaterial shell's dipolar ($n = 1$) and quadrupolar ($n = 2$) resonances. The resonance indicated by higher PR values for $-5 < \mu_{\phi 2} < -3.5$ corresponds to a dipolar mode, whereas the resonance indicated by higher PR values for $-2.5 < \mu_{\phi 2} < -1.5$ corresponds to a quadrupolar mode. As suggested from (11), the PR is significantly increased when $\mu_{\phi 2} < 0$, for which peaks in

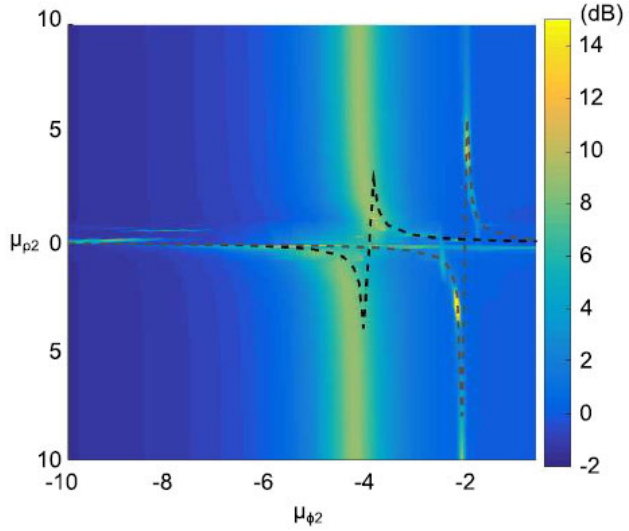

FIGURE 2. The simulated PR as a function of $\mu_{\rho 2}$ and $\mu_{\phi 2}$ for a 2D metamaterial shell with $b = 5$ mm and $a = 3$ mm. The theoretical condition (11) for the dipolar (black-dashed curve) and quadrupolar (grey-dashed curve) resonances is superposed.

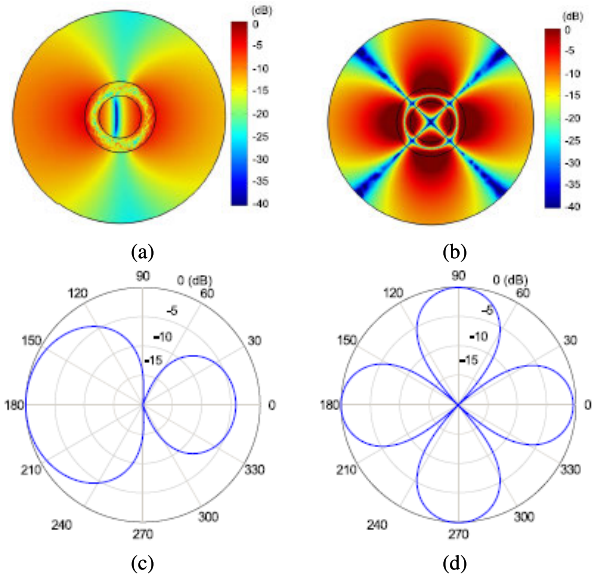

FIGURE 3. The complex electric-field magnitude [radiation pattern] of the metamaterial shell's (a) [c] dipolar and (b) [d] quadrupolar resonances at the optimized values of $\mu_{\rho 2}$ and $\mu_{\phi 2}$ when m is imaginary.

the PR are observed in each figure in two regions: one when $\mu_{\rho 2} > 0$ and m is imaginary, and another when $\mu_{\rho 2} < 0$ and m is real. PR plots obtained for $\mu_{\rho 2} < 0$ and $\mu_{\phi 2}$ values as predicted from (11), by fixing the a/b ratio, show a one-to-one correspondence with the PR plot in Fig. 2 for dipolar (black-dashed curve) and quadrupolar (grey dashed curve) resonances. The simulated PR attains appreciable values of 8.66 dB ($\mu_{\phi 2} = -4.5, \mu_{\rho 2} = -1$) and 9.66 dB ($\mu_{\phi 2} = -3.8, \mu_{\rho 2} = 1$) for the dipolar resonance and 23.5 dB ($\mu_{\phi 2} = -2.39, \mu_{\rho 2} = -1$) and 24 dB ($\mu_{\phi 2} = -1.69, \mu_{\rho 2} = 1$) for the quadrupolar resonance. It should be noted that these PR values deviate slightly from their maximum values due to the approximations employed in (11) and to the choice of a practically sized metamaterial shell. Figs. 3a-3b present the complex electric-field magnitudes at these dipolar and quadrupolar resonances' optimized values of $\mu_{\rho 2}$ and $\mu_{\phi 2}$. Although not shown, the value of $\mu_{\rho 2}$, and as a result m being real or imaginary, has little effect on the near- fields, for which an observable difference occurs only in the interior of the shell. The corresponding radiation patterns in Figs. 3c-3d exhibit the expected dipolar and quadrupolar patterns, respectively.

Inserting a, b, and the simulated optimized values of $\mu_{\rho 2}$ into (11), the resonances are predicted to occur at ($\mu_{\phi 2} = -3.6, \mu_{\rho 2} = 1$) and ($\mu_{\phi 2} = -4.27, \mu_{\rho 2} = -1$) for the dipolar resonance and ($\mu_{\phi 2} = -1.66, \mu_{\rho 2} = 1$) and ($\mu_{\phi 2} = -2.34, \mu_{\rho 2} = -1$) for the quadrupolar resonance. These predicted values of $\mu_{\phi 2}$ are in very close agreement with the simulated optimized values. It is interesting to note that in both (11) and the simulated PR, only $\mu_{\phi 2}$ is required to be negative to effect useful PR enhancement and $\mu_{\rho 2}$ can assume any value. In fact, $\mu_{\phi 2} > 0$ does not effect any PR enhancement (effectively, 0 dB) since the shell's resonances are not excited. One important conclusion from this study is that small variations in negative $\mu_{\phi 2}$ values will degrade the quality of the resonances sharply, whereas $\mu_{\rho 2}$ is more tolerant to such variations.

IV. NUMERICAL STUDY OF 3D ANISOTROPIC SHELLS

The finite height of the antenna and metamaterial shell will now be considered. The simulation model consists of the fully 3D shell and antenna system is depicted in Fig. 1 which is embedded in a vacuum cylinder of height $5d$ and radius $3b$ with PML outer boundaries. Once again, the ELS is modeled using an infinitesimally thin PEC wire directed along the z-axis. Whereas in the previous 2D case the current on the ELS is uniform, in the 3D analysis the current distribution in the z- direction closely follows the well-known sinusoidal distribution of a finite-height dipole with $f(k_z z) = \sin(k_z(d/2 - |z|))$, which achieves a maximum at $z = 0$. To model this response in simulation, the ELS is center-driven by a small wave port. The metamaterial shell's inner and outer radii ($a = 3$ mm and $b = 5$ mm), permittivity $\left(\overline{\overline{\epsilon_2}} = \overline{\overline{I}}(1, 1, 1)\epsilon_0\right)$ and permeability $\left(\overline{\overline{\mu_2}} = \overline{\overline{I}}(\mu_{\phi 2}, \mu_{\rho 2}, 1)\mu_0\right)$ tensors, antenna position ($\rho_s = 2.9$ mm, $\phi_s = 0^o$), and frequency of operation ($f = 3.0$ GHz) are kept consistent with simulations of the 2D (vertically infinite) metamaterial shell in the previous section. The metamaterial shell and antenna are assigned a height $d = \lambda_0/2 = 50$ mm.

The PR as a function of $\mu_{\rho 2}$ and $\mu_{\phi 2}$ are shown in Figs. 4a-4b for 3D metamaterial shells of height $d = \lambda_0/2$ and $d = \lambda_0/10$, respectively. Although the introduction of finite height into the model appears to dampen the PR resonances, the PR curve exhibits a similar trend as compared to the 2D case in Sec. III. For $d = \lambda_0/2$, two PR peaks are observed for each resonant mode: 7 dB (real m) and 7.5 dB

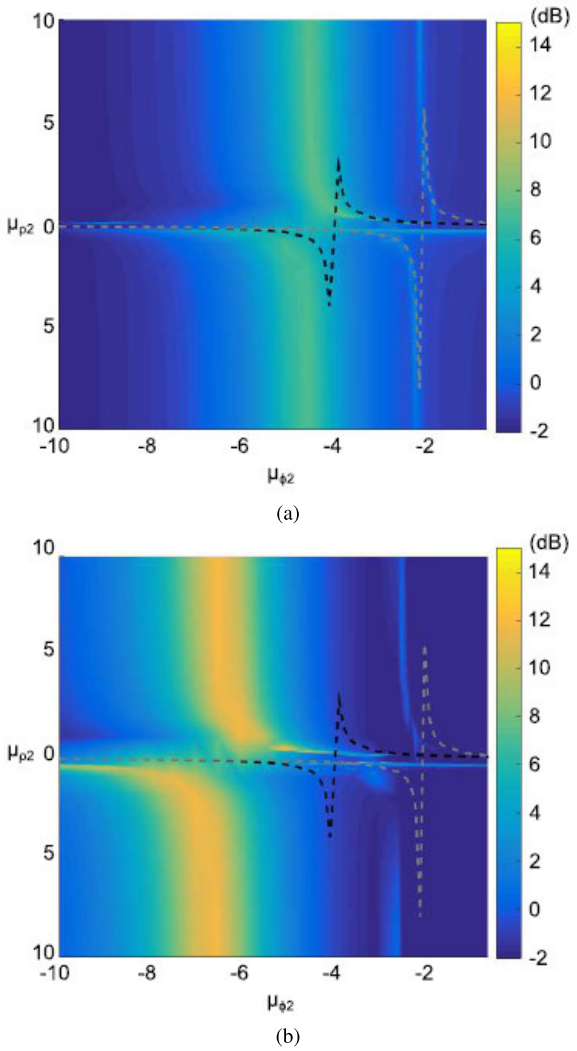

FIGURE 4. The PR as a function of $\mu_{\rho 2}$ and $\mu_{\phi 2}$ for a 3D metamaterial shell of height (a) $d = \lambda_0/2$ and (b) $d = \lambda_0/10$. The theoretical condition (11) of the dipolar (black-dashed curve) and quadrupolar (grey-dashed curve) resonances is superposed.

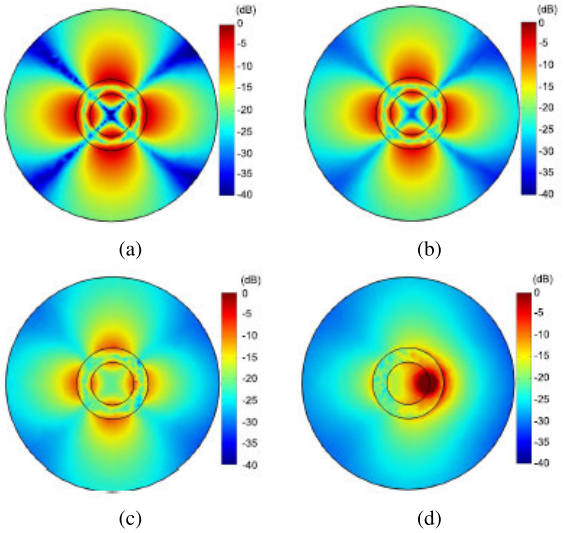

FIGURE 5. Complex electric-field magnitude for the 3D metamaterial shell of height $h = \lambda_0/2$ quadrupolar resonance in the $\rho - \phi$ plane at $z =$ (a) 0, (b) $\lambda_0/8$, (c) $\lambda_0/5$, and (d) $\lambda_0/4$.

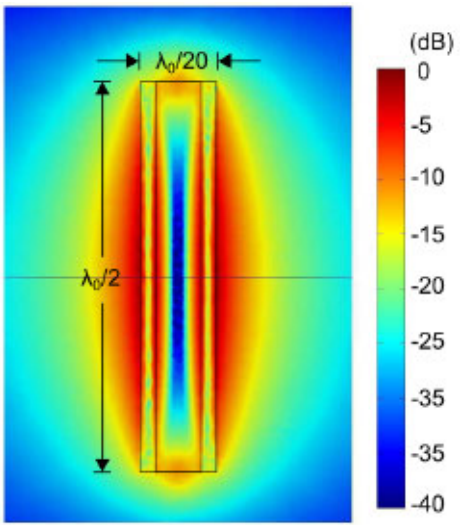

FIGURE 6. Complex electric-field magnitude at the quadrupolar resonance along the ρ-z plane.

(imaginary m) for the dipolar mode and 1.9 dB (real m) and 1.6 dB (imaginary m) for the quadrupolar mode. It should be noted that the quadrupolar mode is extremely sensitive to variation in dimensions and material parameters of the shell, hence its large PR variation as compared to the dipolar mode. Despite the finite height of the antenna, the optimized resonant values of $\mu_{\rho 2}$ and $\mu_{\phi 2}$ are consistent with those predicted by (11) for the previous 2D case. On the other hand, for $d = \lambda_0/10$, it can be seen that the PR's peaks do not correspond to those found from (11). This is attributed to the axial current distribution deviating from our assumed sinusoidal variation and the increasingly dominant fringing fields at the top and bottom edges of the shell. These are less prevalent when $d = \lambda_0/2$ and result in only slight deviation in the simulated and theoretical PR. Nevertheless, it should be noted that the $\lambda_0/10$ anisotropic metamaterial shell enhances the radiated power of the ELS radiator by approximately 14.5 dB (for the dipolar resonance).

Electric-field magnitudes in the ρ-ϕ plane at $z = 0$ for $d = \lambda_0/2$ are shown in Fig. 5a and reveals the typical quadrupolar profile observed in the previous 2D case. Whereas the resonance appears to weaken away from the antenna's center and disappears entirely at the antenna's edge, as shown in Figs. 5b - 5d for $z = \lambda_0/8, \lambda_0/5$, and $\lambda_0/4$ respectively. The decrease in field strength is commensurate with the sinusoidal current variation of the ELS. This axial variation of the fields can be observed in Fig. 6, which presents the normalized complex electric-field magnitudes over the entire height of the metamaterial shell ($\rho - z$ plane). Figs. 5 and 6 also confirm the original assumption that the fields at resonances are confined to the region $|z| \leq d/2$.

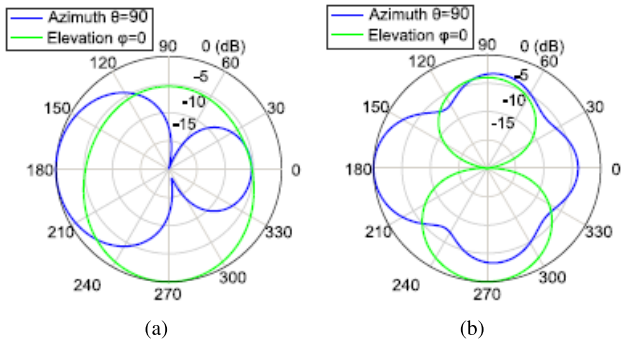

FIGURE 7. The radiation pattern in the azimuth ($\theta = 90^o$) and elevation ($\phi = 90^o$) planes of the 3D metamaterial shell's (a) dipolar and (b) quadrupolar resonances.

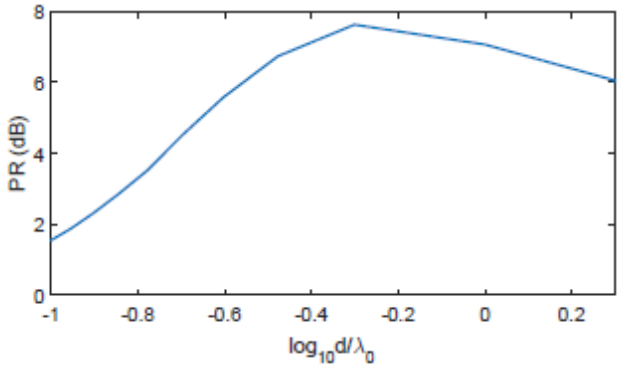

FIGURE 8. PR for the 3D metamaterial shell's dipolar resonance as a function of height, for a fixed outer radius *b*.

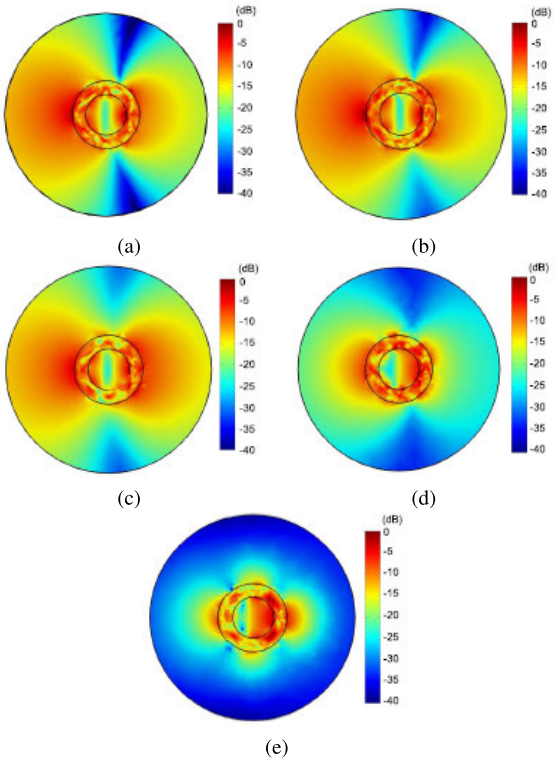

FIGURE 9. Electric-field magnitude in the near field at $z = 0$ for the 3D metamaterial shell of height d = (a) $2\lambda_0$, (b) λ_0, (c)$\lambda_0/2$, (d) $\lambda_0/5$, (e) $\lambda_0/10$.

The introduction of the metamaterial shell alters the expected donut-shaped radiation pattern of the z-directed dipole antenna, which exhibits a null on the z-axis and a maximum in the x-y plane. The blue curves in Figs. 7a-7b present the patterns corresponding to the 3D metamaterial shell's dipolar and quadrupolar resonances, respectively, in the azimuth ($\theta = 90^o$) plane. As expected from the similarity in the 2D and 3D metamaterial shells' near fields, the resonances exhibit the expected dipolar and quadrupolar patterns in the azimuth plane. The radiation patterns in the elevation plane (green curves) ($\phi = 90^o$) of the 3D metamaterial shell's dipolar and quadrupolar resonances are shown in Figs. 7a-7b, respectively. In the elevation plane, the dipolar resonance has a nearly omnidirectional pattern while the quadrupolar resonance has the typical dipole-like pattern.

Fig. 6 clearly demonstrates the metamaterial shell's extremely subwavelength radius when compared to its resonant height. However, in practice it would be useful to reduce the overall size of the metamaterial shell, which leads us to question how small both b and d can be. Fig. 8 presents the PR for the metamaterial shell's dipolar mode as b is maintained, but d varies from being electrically long ($d = 2\lambda_0$) to electrically short ($d = \lambda_0/10$). The PR generally decreases with height and has maximum when ($d = \lambda_0/10$). The complex electric-field magnitudes in the $\rho - \phi$ plane at $z = 0$ for $d = 2\lambda_0, \lambda_0, \lambda_0/2, \lambda_0/5$, and $\lambda_0/10$ are shown in Figs. 9a-9e, respectively, and reveal that the dipolar resonance is still significantly excited for a height as small as $\lambda_0/5$. But it must be noted that all these simulation results are obtained for material parameters obtained from the approximate analytical result given by (11) for a given a/b ratio. Although this result remains valid for a shell with deeply subwavelength radius ($b = \lambda_0/20$), it does not appear to capture resonances for a similar reduction in height. Nevertheless, it is interesting to note that (11) still predicts, with sufficient accuracy, the resonances of an ELS-excited metamaterial shell of finite and subwavelength height, suggesting that the theoretical approximations may still be accurate for useful levels of miniaturization.

Figs. 10a-10b present the radiation patterns of the 3D metamaterial shell of height $d = 2\lambda_0$ and $d = \lambda_0/10$, respectively, in the azimuth (blue curve) and elevation (green curve) planes. Whereas changing the height of the shell leaves the azimuth plane's radiation pattern unchanged, increasing height results in more axial variation of the current which is clearly seen in the elevation plane.

It is worth reminding the reader that due to the hybrid nature of the modes in the fully 3D geometry, all tensor elements of the permittivity and permeability would generally need to be accounted for. However, this work is focused in using the z-directed ELS to exclusively excite the metamaterial shell's *TM* mode resonances, for which the theory presented in Sec. II predicts only $\mu_{\rho 2}$ and $\mu_{\phi 2}$ are implicated.

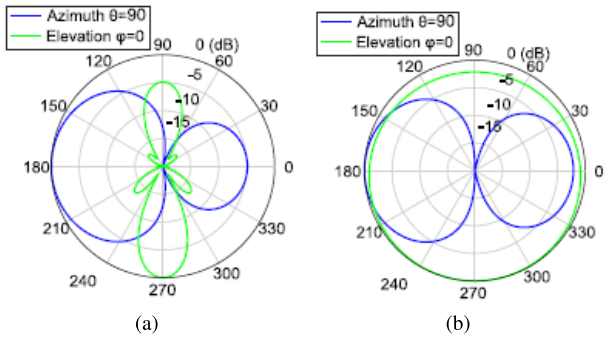

FIGURE 10. The radiation pattern in the azimuth ($\theta = 90^o$) and elevation ($\phi = 0^o$) planes for the 3D metamaterial shell of height (a) $d = 2\lambda_0$ and (b) $d = \lambda_0/10$ normalized to their respective maximum value.

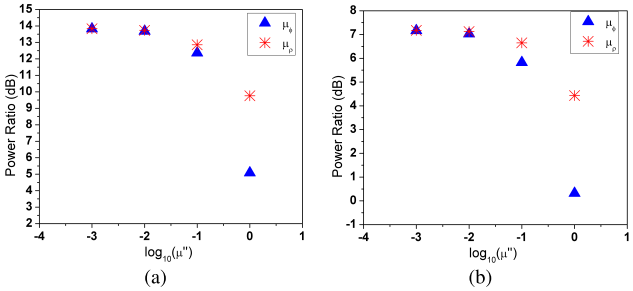

FIGURE 11. Study of loss with variation of imaginary component of effective permeability (a) d = $\lambda_0/10$ and (b) d = $\lambda_0/2$.

In order to practically implement such a 3D shell for radiation enhancement, metamaterial structures with biaxial anisotropy need to be considered. Practical implementations of such anisotropy are available in the so-called transmission-line metamaterials, which are well-studied [28], [29]. For the proposed shells, a cylindrical arrangement of such metamaterials cells can be used to achieve the desired anisotropic physical parameters. One such method is demonstrated in [17], where radially oriented negative refractive index transmission line (NRI-TL) metamaterials are arranged azimuthally and excited by an electric line source (ELS) placed near the outer boundary of the metamaterial shell to obtain a radiation enhancement. The fields of the ELS appear anisotropic in the azimuthal and radial direction for such a metamaterial cylinder. In order to implement a structure with $\lambda/2$ height as reported in the current work, azimuthally arranged NRI-TL structures can be stacked vertically along the height of the antenna, with antenna placed in the vicinity of metamaterial cylinder. But the thickness of the structure reported in [17] is around $\lambda/18$. As the resonances are strongly dependent on thickness of the shell, studies must be carried out to implement such structures with smaller thickness, to improve the PR; fortunately, transmission-line metamaterials are highly amenable to reduced sizes using strong discrete lumped reactive loading.. Another method to implement 3D radiation enhancement is by azimuthal arrangement of double- sided SRR structures, as shown in [5]. But for such resonating

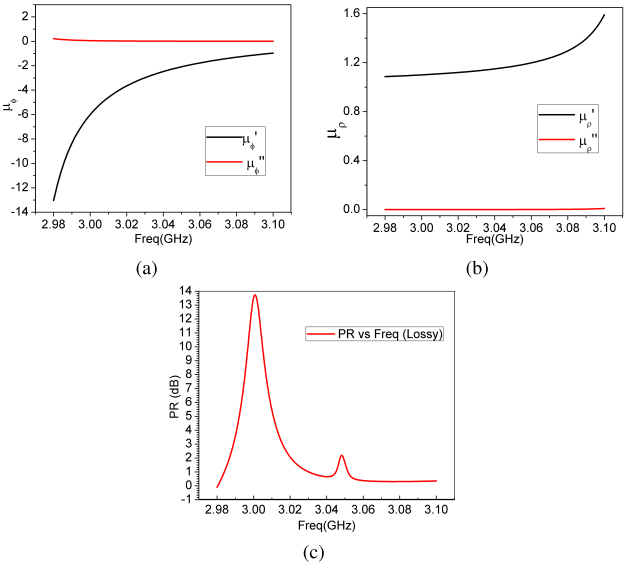

FIGURE 12. Lossy dispersive model. (a) μ_ρ, (b) μ_ϕ, (c) and PR versus frequency.

structures, as MNG characteristics are obtained for only a narrow frequency range, control of design parameters may be challenging.

V. EFFECT OF DISPERSION AND LOSS

Causality constraints require that negative material parameters be accompanied by physically appropriate frequency dispersion, and the question of loss naturally arises in resonant phenomena. In the present work, it is important to establish the effect of dispersion and loss of the anisotropic metamaterial structure on the resonant PR enhancement spectrum. For this purpose, a 3D anisotropic metamaterial shell with height $\lambda_0/10$ is considered. For lossy structures the effective medium tensor components are complex in nature which is given $\mu_\phi = \mu'_\phi - j\mu''_\phi$ and $\mu_\rho = \mu'_\rho - j\mu''_\rho$, where μ''_ϕ and μ''_ρ represent loss.

To understand the effects of loss, the imaginary component of μ_ϕ and μ_ρ are varied in decades from $\mu'' = 0.001$ to $\mu'' = 1$ as represented in Fig. 11. For a structure with $d = \lambda_0/10$, as shown in Fig.11a, variation of $\mu''_{\phi 2}$ is obtained by keeping $\mu_{\rho 2} = \mu'_{\rho 2} = 1.1$, where as variation of $\mu''_{\rho 2}$ by considering $\mu_{\phi 2} = \mu'_{\phi 2} = -6$. In the previous section, it was observed that variation in $\mu'_{\phi 2}$ degrades the quality of the resonance sharply, and more so than does variation in $\mu'_{\rho 2}$. Similarly, here it can be observed that losses introduced via $\mu''_{\phi 2}$ have a much more deleterious effect on the resonance than do losses introduced via $\mu''_{\rho 2}$. A similar trend is observed with a metamaterial shell height of $d = \lambda_0/2$, as shown in Fig.11b. Fig. 11b also shows that, there is no significant degradation of PR, suggesting that (11) is effective at providing an approximate solution even in the presence of moderate losses. However, as can be seen in Fig.11, with addition of more losses the resonances die out and the enhancement in radiation is compromised.

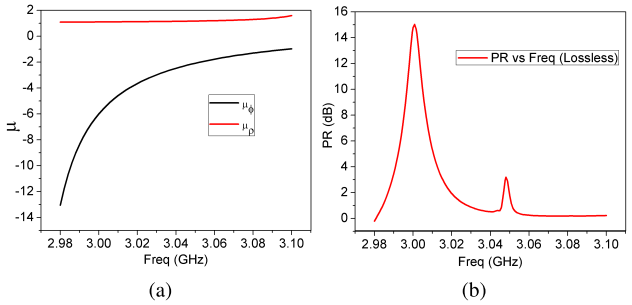

FIGURE 13. Lossless dispersive model. (a) μ_ρ and μ_ϕ, and (b) PR versus frequency.

Fig. 4 showed that a structure with height $d = \lambda_0/10$ provides a PR of around 14 dB for $\mu_{\phi 2} = -6$. To further study the effect of dispersion with loss on the resonances of the metamaterial structure, the relative effective permeabilities, $\mu_{\phi 2}$ and $\mu_{\rho 2}$ in region 2 of Fig.1, each imbued with a lossy Lorentz dispersion profile given by the expression

$$\mu(\omega) = \left(1 - \frac{\omega_{pm}^2}{\omega^2 - \omega_{mr}^2 - j\Gamma_m\omega}\right) \tag{14}$$

where, ω_{pm} and ω_{mr} are the magnetic plasma frequency and resonance frequency, respectively. Γ_m is the magnetic collision frequency providing the loss. The parameters of this dispersion model are chosen to recover $\mu'_{\phi 2} = -6$ and $\mu'_{\rho 2} = 1.1$ at a frequency of operation $f = 3.0$ GHz. The magnetic collision frequency is chosen as $\Gamma_m = 4\times10^6$ rad/s in order to simulate loss values that are typical of practical metamaterials [27]. From the Lorentz model shown in (14), it is evident that the frequency of operation ($\omega = 2\pi f$) must generally lie in the range $\omega_{mr} < \omega < \omega_{mp}$ to obtain the required negative value of $\mu'_{\phi 2}$. As such, the magnetic resonance frequency is chosen as $\omega_{mr\phi} = 2\pi \times 2.96$ GHz. Similarly, to obtain the required positive value of $\mu'_{\rho 2}$, $\omega_{mr\rho} = 2\pi \times 3.12$ GHz is chosen. For these given values, the azimuthal and radial effective permeabilities are obtained as $\mu_{\phi 2} = -6 - j0.057$ and $\mu_{\rho 2} = 1.1 - j0.001$ at $f = 3.0$ GHz. To independently establish the effects of dispersion versus loss, the corresponding lossless case ($\Gamma_m = 0$) is also considered for comparison.

Figs. 12 and 13 show the PR spectrum obtained using the lossy and lossless dispersion models, respectively. Two peaks are observed in both cases. The peak obtained at 3.0 GHz represents a dipolar resonance while the second peak at 3.048 GHz represents quadrupolar resonance. The electric-field magnitudes at these resonances in both the lossy and lossless cases are shown in Fig. 14. The introduction of practical losses, result in only 1 dB reduction of PR at the dipolar resonance, and only 0.5 dB at the quadrupolar resonance. This shows that the proposed anisotropic metamaterial shell can contribute a significant amount of radiation enhancement even in the presence of practical metamaterial losses.

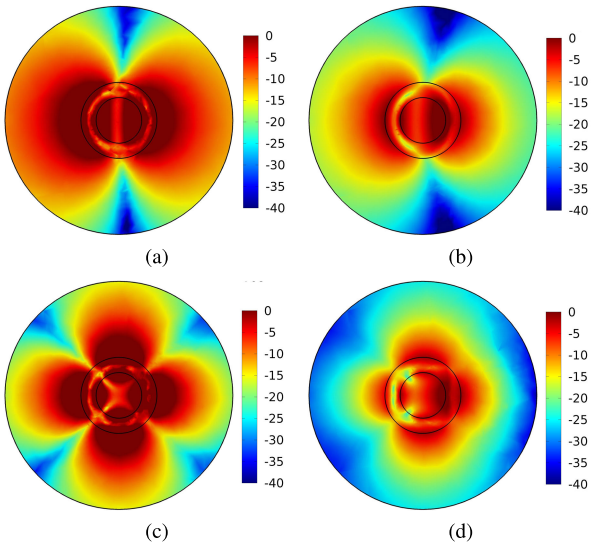

FIGURE 14. Complex electric field magnitude in ρ-ϕ plane for (a) dipolar resonance for lossless case ($f = 3$ GHz) (b) dipolar resonance for lossy case ($f = 3$ GHz) (c) quadrupolar resonance for lossless case ($f = 3.048$ GHz) (d) quadrupolar resonance for lossy case ($f = 3.048$ GHz).

VI. CONCLUSION

This paper has presented an analytical and numerical study of cylindrical metamaterial shells possessing cylindrically anisotropic permeability, which are excited by an ELS. It was shown that an ELS will excite resonances in the metamaterial shell that contribute to significant enhancements in radiated power and scattering of the fields into well-known resonant field profiles. An analytical resonance condition predicts that only the azimuthal component of the permeability tensor need assume negative values to effect significant miniaturization of the shell's radius. This is shown to be accurate through comparison with full-wave simulations of 2D and 3D metamaterial shells. The analytical formulation is also found to accurately predict the resonant response of the 3D metamaterial shell, which exhibits resonances with useful PR enhancements provided the shell's height is not electrically very small. A loss and dispersion analysis is also carried out, and it is observed that the introduction of loss in the azimuthal component of the permeability tensor affects the PR spectrum more significantly than does that in the radial component. Further dispersion analysis assuming a lossy Lorentz model shows that, for practical metamaterial losses, PR is not significantly reduced from lossless case.

REFERENCES

[1] S. Enoch, G. Tayeb, P. Sabouroux, N. Guérin, and P. Vincent, "A metamaterial for directive emission," *Phys. Rev. Lett.*, vol. 89, no. 21, Nov. 2002, Art. no. 213902.
[2] Y. G. Ma, P. Wang, X. Chen, and C. K. Ong, "Near-field plane-wave-like beam emitting antenna fabricated by anisotropic metamaterial," *Appl. Phys. Lett.*, vol. 94, no. 4, Jan. 2009, Art. no. 044107.
[3] Q. Cheng, W. X. Jiang, and T. J. Cui, "Radiation of planar electromagnetic waves by a line source in anisotropic metamaterials," *J. Phys. D, Appl. Phys.*, vol. 43, no. 33, Aug. 2010, Art. no. 335406.

[4] Y. He, N. Ding, L. Zhang, W. Zhang, and B. Du, "Short–length and high-aperture-efficiency horn antenna using low–loss bulk anisotropic metamaterial," *IEEE Antennas Wireless Propag. Lett.*, vol. 14, pp. 1642–1645, 2015.
[5] A. Dadgarpour, A. A. Kishk, and T. A. Denidni, "Gain enhancement of planar antenna enabled by array of split–ring resonators," *IEEE Trans. Antennas Propag.*, vol. 64, no. 8, pp. 3682–3687, Aug. 2016.
[6] J. Xiong, Y. Hu, S. Mao, W. Zhang, S. Xiao, and B.-Z. Wang, "Agile beamwidth control and directivity enhancement for aperture radiation with low–profile metasurfaces," *IEEE Trans. Antennas Propag.*, vol. 66, no. 3, pp. 1528–1533, Mar. 2018.
[7] S. Zhu, H. Liu, and P. Wen, "A new method for achieving miniaturization and gain enhancement of Vivaldi antenna array based on anisotropic metasurface," *IEEE Trans. Antennas Propag.*, vol. 67, no. 3, pp. 1952–1956, Mar. 2019.
[8] Z. H. Jiang, L. Kang, and D. H. Werner, "Conformal metasurface-coated dielectric waveguides for highly confined broadband optical activity with simultaneous low-visibility and reduced crosstalk," *Nature Commun.*, vol. 8, no. 1, p. 356, Dec. 2017.
[9] H. Jiang, L.-M. Si, W. Hu, and X. Lv, "A symmetrical dual–beam bowtie antenna with gain enhancement using metamaterial for 5G MIMO applications," *IEEE Photon. J.*, vol. 11, no. 1, pp. 1–9, Feb. 2019.
[10] A. K. Singh, M. P. Abegaonkar, and S. K. Koul, "A negative index metamaterial lens for antenna gain enhancement," in *Proc. Int. Symp. Antennas Propag. (ISAP)*, Oct. 2017, pp. 1–2.
[11] A. Monti, J. Soric, A. Alu, F. Bilotti, A. Toscano, and L. Vegni, "Overcoming mutual blockage between neighboring dipole antennas using a low–profile patterned metasurface," *IEEE Antennas Wireless Propag. Lett.*, vol. 11, pp. 1414–1417, 2012.
[12] Z. Haider, M. U. Khan, and H. M. Cheema, "A dual–band metamaterial superstrate for antenna gain enhancement," in *Proc. IEEE Int. Symp. Antennas Propag. USNC/URSI Nat. Radio Sci. Meeting*, Boston, MA, USA, Jul. 2018, pp. 1017–1018.
[13] R. Ziolkowski and A. Kipple, "Application of double negative materials to increase the power radiated by electrically small antennas," *IEEE Trans. Antennas Propag.*, vol. 51, no. 10, pp. 2626–2640, Oct. 2003.
[14] N. Wang, H. Chen, W. Lu, S. Liu, and Z. Lin, "Giant omnidirectional radiation enhancement via radially anisotropic zero-index metamaterial," *Opt. Express*, vol. 21, no. 20, p. 23712, Oct. 2013.
[15] D. Mitra, S. Paul, D. Bhattacharya, and S. R. Bhadra Chaudhuri, "Radiated power enhancement of quadrupole source using metamaterials," *Microw. Opt. Technol. Lett.*, vol. 55, no. 11, pp. 2620–2624, Nov. 2013.
[16] S. Arslanagic, R. W. Ziolkowski, and O. Breinbjerg, "Analytical and numerical investigation of the radiation and scattering from concentric metamaterial cylinders excited by an electric line source," *Radio Sci.*, vol. 42, no. 6, pp. 1–22, Dec. 2007.
[17] J. G. Pollock and A. K. Iyer, "Effective–medium properties of cylindrical transmission–line metamaterials," *IEEE Antennas Wireless Propag. Lett.*, vol. 10, pp. 1491–1494, 2011.
[18] J. A. Hodge, T. Anthony, and A. I. Zaghloul, "Enhancement of the dipole antenna using a capcitively loaded loop (CLL) structure," in *Proc. IEEE Antennas Propag. Soc. Int. Symp. (APSURSI)*, Jul. 2014, pp. 1544–1545.
[19] J. Carbonell, D. Torrent, and J. Sanchez-Dehesa, "Radial photonic crystal shells and their application as resonant and radiating elements," *IEEE Trans. Antennas Propag.*, vol. 61, no. 2, pp. 755–767, Feb. 2013.
[20] J. G. Pollock and A. K. Iyer, "Experimental verification of below–cutoff propagation in miniaturized circular waveguides using anisotropic ENNZ metamaterial liners," *IEEE Trans. Microw. Theory Techn.*, vol. 64, no. 4, pp. 1297–1305, Apr. 2016.
[21] S. Arslanagic, R. W. Ziolkowski, and O. Breinbjerg, "Analytical and numerical investigation of the radiation from concentric metamaterial spheres excited by an electric Hertzian dipole," *Radio Sci.*, vol. 42, no. 6, pp. 1–20, Dec. 2007.
[22] S. Long, M. Mcallister, and L. Shen, "The resonant cylindrical dielectric cavity antenna," *IEEE Trans. Antennas Propag.*, vol. AP-31, no. 3, pp. 406–412, May 1983.
[23] J. C. Soric, N. Engheta, S. Maci, and A. Alu, "Omnidirectional metamaterial antennas based on ε-near-zero channel matching," *IEEE Trans. Antennas Propag.*, vol. 61, no. 1, pp. 33–44, Jan. 2013.
[24] D. Kajfez,*Dielectric Resonators*. Norwood, MA, USA: Artech House, 1986, pp. 113–184.
[25] J. Sheen, "Time harmonic electromagnetic fields in an biaxial anisotropic medium," *J. Electromagn. Waves Appl.*, vol. 19, no. 6, pp. 753–767, Jan. 2005.
[26] *COMSOL Verision 5*, COMSOL, Stockholm, Sweden, 2016.
[27] A. K. Iyer and G. V. Eleftheriades, "Free–space imaging beyond the diffraction limit using a veselago–pendry transmission–line metamaterial superlens," *IEEE Trans. Antennas Propag.*, vol. 57, no. 6, pp. 1720–1727, Jun. 2009.
[28] A. K. Iyer and G. V. Eleftheriades, "Volumetric layered transmission-line metamaterial exhibiting a negative refractive index," *J. Opt. Soc. Amer. B, Opt. Phys.*, vol. 23, no. 3, pp. 553–570, Mar. 2006.
[29] A. Iyer, K. Balmain, and G. Eleftheriades, "Dispersion analysis of resonance cone behaviour in magnetically anisotropic transmission-line metamaterials," in *IEEE Antennas Propag. Soc. Symp. Dig.*, Monterey, CA, USA, Jun. 2004, pp. 3147–3150.

R. ANEESH KUMAR (Member, IEEE) received the B.Tech. degree in electronics and communications from Kerala University, Thiruvananthapuram, Kerala, India, in 2006, and the M.Tech. degree in RF and microwave from the Indian Institute of Space Science and Technology (IIST), Thiruvananthapuram, in 2016, where he is currently pursuing the Ph.D. degree.

He has joined as an Engineer with ISRO Telemetry, Tracking and Command Network (ISTRAC), Bengaluru under Indian Space Reasearch Organisation (ISRO), in 2008, where he was working on design and development of microwave transmitters for radar systems. He has been with the Vikram Sarabhai Space Centre (VSSC), Thiruvananthapuram under ISRO, since 2011, where he is also working on instrumentation systems. His research interests include wireless instrumentation, antennas, microwave circuit design, rectennas, and electromagnetic energy harvesting.

JUSTIN G. POLLOCK (Member, IEEE) received the B.A.Sc. (Hons.) and Ph.D. degrees in electrical engineering from the Department of Electrical and Computer Engineering, University of Alberta, Edmonton, AB, Canada, in 2011 and 2016, respectively, with an emphasis on the theory and applications of cylindrical metamaterial waveguides and antennas.

He is currently a Senior Antenna Engineer in KP Performance Antennas Inc., Edmonton, AB, Canada, where he leads the design of telecommunication antenna systems for the fixed wireless, microwave backhaul, last-mile connectivity, and cellular markets.

CHINMOY SAHA (Senior Member, IEEE) received the B.Tech., M.Tech., and Ph.D. degrees in radio physics and electronics from the University of Calcutta, Kolkata, India, in 2002, 2005, and 2012, respectively.

He is currently working as an Associate Professor with the Department of Avionics, Indian Institute of Space Science and Technology, under the Department of Space, Government of India. He has visited several International Universities of repute like the Royal Military College of Canada (RMC), Kingston, ON, Queens University in various capacities and having collaborative research with RMC Canada. His current research interests include microwave circuits, engineered materials, metamaterial inspired antennas and circuits, reconfigurable and multifunctional antennas for modern wireless applications, dielectric resonator antennas, and THz antennas. He has more than ninety publications in peer reviewed national and international journals and conference proceedings, and has authored two books with Cambridge University Press, U.K., and Taylor and Francis, USA.

Dr. Saha is a Life Member of IETE. He is currently the Chairman of Antennas and Propagation Chapter of the IEEE Kerala Section. He is also the founding and current Chairman of the IEEE MTT-S Kerala Chapter. He has received several prestigious awards, which includes National Scholarship from Ministry of Human Resource Development from Government of India, the Outstanding Contribution Award from the AP-MTT Kolkata Chapter, the Best Contribution Award for Notable Services and Significant Contributions towards the Advancements of the IEEE and the Engineering Profession from the IEEE Kolkata Section and several best paper awards in various International conferences. He is on the board of reviewers of several international journals of repute, including the IEEE TRANSACTIONS ON ANTENNAS AND PROPAGATION, the IEEE ANTENNAS AND WIRELESS PROPAGATION LETTERS (IEEE AWPL), *IET Microwaves, Antennas and Propagation*, *Electronic Letters*, and *Nature Scientific Reports*.

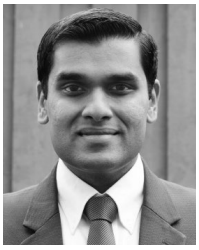

ASHWIN K. IYER (Senior Member, IEEE) received the B.A.Sc., M.A.Sc., and Ph.D. degrees in electrical engineering from the University of Toronto, Toronto, ON, Canada, in 2001, 2003, and 2009, respectively, with a focus on the discovery and development of the negative-refractive-index transmission-line approach to metamaterial design and the realization of metamaterial lenses for free-space microwave subdiffraction imaging.

He is currently an Associate Professor with the Department of Electrical and Computer Engineering, University of Alberta, Edmonton, AB, Canada, where he leads a team of graduate students investigating novel RF/microwave circuits and techniques, fundamental electromagnetic theory, antennas, and engineered metamaterials, with an emphasis on their applications to microwave and optical devices, defense technologies, and biomedicine. He has coauthored a number of highly cited articles and book chapters on the subject of metamaterials.

Dr. Iyer is a member of the IEEE AP-S Education Committee and a Registered Member of the Association of Professional Engineers and Geoscientists of Alberta. He was a recipient of the IEEE AP-S R. W. P. King Award, in 2008, the IEEE AP-S Donald G. Dudley Jr. Undergraduate Teaching Award, in 2015, the University of Alberta Provost's Award for Early Achievement of Excellence in Undergraduate Teaching, in 2014, and the University of Alberta Rutherford Award for Excellence in Undergraduate Teaching, in 2018. His students are the recipients of several major national and international awards for their research. He serves as the Co-Chair for the IEEE Northern Canada Section's Award-Winning Joint Chapter of the AP-S and MTT-S societies and a Technical Program Committee Co-Chair for the 2020 AP-S/URSI International Symposium. From 2012 to 2018, he was an Associate Editor of the IEEE TRANSACTIONS ON ANTENNAS AND PROPAGATION, where he currently serves as a Track Editor. He is also the Guest Editor of the IEEE TRANSACTIONS ON ANTENNAS AND PROPAGATION Special Issue on Recent Advances in Metamaterials and Metasurfaces.